

Observations of the Sagittarius Dwarf galaxy by the H.E.S.S. experiment and search for a Dark Matter signal

F. Aharonian¹, A.G. Akhperjanian², A.R. Bazer-Bachi³,
M. Beilicke⁴, W. Benbow¹, D. Berge^{1,a}, K. Bernlöhr^{1,5},
C. Boisson⁶, O. Bolz¹, V. Borrel³, I. Braun¹, E. Brion⁷,
A.M. Brown⁸, R. Bühler¹, I. Büsching⁹, T. Boutelier¹⁷,
S. Carrigan¹, P.M. Chadwick⁸, L.-M. Chounet¹⁰,
G. Coignet¹¹, R. Cornils⁴, L. Costamante^{1,23}, B. Degrang¹⁰,
H.J. Dickinson⁸, A. Djannati-Atai¹², L.O'C. Drury¹³,
G. Dubus¹⁰, K. Egberts¹, D. Emmanoulopoulos¹⁴,
P. Espigat¹², C. Farnier¹⁵, F. Feinstein¹⁵, E. Ferrero¹⁴,
A. Fiasson¹⁵, G. Fontaine¹⁰, Seb. Funk⁵, S. Funk¹,
M. Füßling⁵, Y.A. Gallant¹⁵, B. Giebels¹⁰, J.F. Glicenstein⁷,
B. Glück¹⁶, P. Goret⁷, C. Hadjichristidis⁸, D. Hauser¹,
M. Hauser¹⁴, G. Heinzelmann⁴, G. Henri¹⁷, G. Hermann¹,
J.A. Hinton^{1,14,b}, A. Hoffmann¹⁸, W. Hofmann¹,
M. Holleran⁹, S. Hoppe¹, D. Horns¹⁸, A. Jacholkowska¹⁵,
O.C. de Jager⁹, E. Kendziorra¹⁸, M. Kerschhaggl⁵,
B. Khélifi^{10,1}, Nu. Komin¹⁵, K. Kosack¹, G. Lamanna¹¹,
I.J. Latham⁸, R. Le Gallou⁸, A. Lemièr¹²,
M. Lemoine-Goumard¹⁰, T. Lohse⁵, J.M. Martin⁶,
O. Martineau-Huynh¹⁹, A. Marcowith^{3,15}, C. Masterson^{1,23},
G. Maurin¹², T.J.L. McComb⁸, E. Moulin^{15,7,*},
M. de Naurois¹⁹, D. Nedbal²⁰, S.J. Nolan⁸, A. Noutsos⁸,
E. Nuss^{15,c}, J-P. Olive³, K.J. Orford⁸, J.L. Osborne⁸,
M. Panter¹, G. Pelletier¹⁷, P.-O. Petrucci¹⁷, S. Pita¹²,
G. Pühlhofer¹⁴, M. Punch¹², S. Ranchon¹¹,
B.C. Raubenheimer⁹, M. Raue⁴, S.M. Rayner⁸, J. Ripken⁴,
L. Rob²⁰, L. Rolland⁷, S. Rosier-Lees¹¹, G. Rowell^{1,d},
V. Sahakian², A. Santangelo¹⁸, L. Saugé¹⁷, S. Schlenker⁵,
R. Schlickeiser²¹, R. Schröder²¹, U. Schwanke⁵,
S. Schwarzburg¹⁸, S. Schwemmer¹⁴, A. Shalchi²¹, H. Sol⁶,
D. Spangler⁸, F. Spanier²¹, R. Steenkamp²², C. Stegmann¹⁶,
G. Superina¹⁰, P.H. Tam¹⁴, J.-P. Tavernet¹⁹, R. Terrier¹²,
M. Tluczykont^{10,23}, C. van Eldik¹, G. Vasileiadis¹⁵,
C. Venter⁹, J.P. Vialle¹¹, P. Vincent¹⁹, M. Vivier⁷,
H.J. Völk¹, S.J. Wagner¹⁴, M. Ward⁸

* Corresponding author : moulin@in2p3.fr; DAPNIA/DSM/CEA, CE Saclay, F-91191 Gif-sur-Yvette Cedex, France

¹ *Max-Planck-Institut für Kernphysik, P.O. Box 103980, D 69029 Heidelberg, Germany*

² *Yerevan Physics Institute, 2 Alikhanian Brothers St., 375036 Yerevan, Armenia*

³ *Centre d'Etude Spatiale des Rayonnements, CNRS/UPS, 9 av. du Colonel Roche, BP 4346, F-31029 Toulouse Cedex 4, France*

⁴ *Universität Hamburg, Institut für Experimentalphysik, Luruper Chaussee 149, D 22761 Hamburg, Germany*

⁵ *Institut für Physik, Humboldt-Universität zu Berlin, Newtonstr. 15, D 12489 Berlin, Germany*

⁶ *LUTH, UMR 8102 du CNRS, Observatoire de Paris, Section de Meudon, F-92195 Meudon Cedex, France*

⁷ *DAPNIA/DSM/CEA, CE Saclay, F-91191 Gif-sur-Yvette, Cedex, France*

⁸ *University of Durham, Department of Physics, South Road, Durham DH1 3LE, U.K.*

⁹ *Unit for Space Physics, North-West University, Potchefstroom 2520, South Africa*

¹⁰ *Laboratoire Leprince-Ringuet, IN2P3/CNRS, Ecole Polytechnique, F-91128 Palaiseau, France*

¹¹ *Laboratoire d'Annecy-le-Vieux de Physique des Particules, IN2P3/CNRS, 9 Chemin de Bellevue - BP 110 F-74941 Annecy-le-Vieux Cedex, France*

¹² *APC, 11 Place Marcelin Berthelot, F-75231 Paris Cedex 05, France[†]*

¹³ *Dublin Institute for Advanced Studies, 5 Merrion Square, Dublin 2, Ireland*

¹⁴ *Landessternwarte, Universität Heidelberg, Königstuhl, D 69117 Heidelberg, Germany*

¹⁵ *Laboratoire de Physique Théorique et Astroparticules, IN2P3/CNRS, Université Montpellier II, CC 70, Place Eugène Bataillon, F-34095 Montpellier Cedex 5, France*

¹⁶ *Universität Erlangen-Nürnberg, Physikalisches Institut, Erwin-Rommel-Str. 1, D 91058 Erlangen, Germany*

¹⁷ *Laboratoire d'Astrophysique de Grenoble, INSU/CNRS, Université Joseph Fourier, BP 53, F-38041 Grenoble Cedex 9, France*

¹⁸ *Institut für Astronomie und Astrophysik, Universität Tübingen, Sand 1, D 72076 Tübingen, Germany*

¹⁹ *LPNHE, Université Pierre et Marie Curie Paris 6, Université Denis Diderot Paris 7, CNRS/IN2P3, 4 Place Jussieu, F-75252 Paris Cedex 5, France*

²⁰ *Institute of Particle and Nuclear Physics, Charles University, V Holesovickach 2, 180 00 Prague 8, Czech Republic*

²¹ *Institut für Theoretische Physik, Lehrstuhl IV: Weltraum und Astrophysik,*

Ruhr-Universität Bochum, D 44780 Bochum, Germany

²² *University of Namibia, Private Bag 13301, Windhoek, Namibia*

²³ *European Associated Laboratory for Gamma-Ray Astronomy, jointly supported by CNRS and MPG*

^a *now at CERN, Geneva, Switzerland*

^b *now at School of Physics & Astronomy, University of Leeds, Leeds LS2 9JT, UK*

^c *not a H.E.S.S. member*

^d *now at School of Chemistry & Physics, University of Adelaide, Adelaide 5005, Australia*

[†] *UMR 7164 (CNRS, Université Paris VII, CEA, Observatoire de Paris)*

Abstract

Observations of the Sagittarius dwarf spheroidal (Sgr dSph) galaxy were carried out with the H.E.S.S. array of four imaging air Cherenkov telescopes in June 2006. A total of 11 hours of high quality data are available after data selection. There is no evidence for a very high energy γ -ray signal above the energy threshold at the target position. A 95% C.L. flux limit of $3.6 \times 10^{-12} \text{cm}^{-2} \text{s}^{-1}$ above 250 GeV has been derived. Constraints on the velocity-weighted cross section $\langle\sigma v\rangle$ are calculated in the framework of Dark Matter particle annihilation using realistic models for the Dark Matter halo profile of Sagittarius dwarf galaxy. Two different models have been investigated encompassing a large class of halo types. A 95% C.L. exclusion limit on $\langle\sigma v\rangle$ of the order of $2 \times 10^{-25} \text{cm}^3 \text{s}^{-1}$ is obtained for a core profile in the 100 GeV - 1 TeV neutralino mass range.

Key words: Gamma-rays : observations - Dwarf Spheroidal galaxy, Dark Matter
PACS : 98.70.Rz, 98.56.Wm, 95.35.+d

1 Introduction

Astrophysical and cosmological observations provide a substantial body of evidences for the existence of Cold Dark Matter (CDM) although its nature remains still unknown. It is commonly assumed that CDM is composed of yet undiscovered non-baryonic particles for which plausible candidates are Weakly Interacting Massive Particles (WIMPs). In most theories, candidates for CDM are predicted in theories beyond the Standard Model of particle physics [1]. The indirect detection of Dark Matter (DM) annihilation may bring new insights to probe the astrophysical nature of Dark Matter. To a large extent complementary to direct searches, the indirect detection enables to search for DM outside the solar system. Indeed, it may give detailed morphology features that may constrain the DM halo profile. The annihilation of WIMPs into γ -rays may lead to detectable very high energy (VHE, $E > 100$ GeV) γ -ray fluxes above background via continuum emission from hadronization of gauge bosons and heavy quarks, or γ -ray lines through loop-induced processes. The H.E.S.S. (High Energy Stereoscopic System) array of Imaging Atmospheric Cherenkov Telescopes (IACTs), designed for high sensitivity measurements in the 100 GeV - 10 TeV energy regime, is a suitable instrument to detect VHE γ -rays and investigate their possible origin.

Various astrophysical systems ranging from local objects in the galactic halo to galaxy cluster scales have been considered as targets for DM annihilation γ -ray studies. Interacting with baryonic matter only through gravity, the WIMPs are expected to concentrate at the centre of high density region. A probable candidate is the elliptical galaxy M87 at the centre of the Virgo cluster [2]. However, the temporal variability of the H.E.S.S. signal [3] excludes the bulk of the signal in the TeV range to be of a dark matter origin. Prospects of indirect detection from the Andromeda galaxy M31 [4] and the Large Magellanic Cloud [5] have been also investigated. H.E.S.S. observations in the direction of the Galactic Center (GC) have revealed a source of VHE γ -ray emission (HESS J1745-290). The measured spectrum is difficult to reconcile with a DM interpretation and does not match the expected annihilation spectrum. The very high energy cut-off above 7 TeV requires an uncomfortably massive DM particle [6]. Moreover, standard astrophysical objects found in the region such as the supermassive black hole Sgr A* or the recently discovered pleion G359.95-0.04, can easily account for the observed signal. The shell-type supernova remnant Sgr A East is unlikely to be associated to the signal [7]. Besides HESS J1745-290, the deep observations carried out with H.E.S.S. in the GC region have highlighted the existence of a diffuse component along the galactic ridge [8]. This extended TeV emission may be explained by cosmic ray interactions inside the central molecular zone leading to diffuse astrophysical backgrounds that might hide the exotic signal [9]. Future indirect DM searches in this region will have to overcome this challenging background. In contrast, dwarf galaxies may be a less complex environment because of the

reduced amount of gas in such small systems [10].

Dwarf Spheroidal galaxies (dSph) such as Sagittarius dwarf or Canis Major, discovered recently in the Local Group, are among the most extreme DM-dominated environments. Indeed, measurements of roughly constant radial velocity dispersion of stars imply large mass to luminosity ratios [11]. Nearby dwarfs are ideal astrophysical probes of the nature of DM as they usually consist of a stellar population with no hot or warm gas, no cosmic ray population and little dust. The Sagittarius dwarf Spheroidal galaxy (Sgr dSph) is the next-to-last Galactic satellite galaxy discovered [12]. The core of Sgr dSph is located at $l = 5.6^\circ$ and $b = -14^\circ$ in galactic coordinates at a distance of about 24 kpc from the Sun [13]. Sgr dSph has made at least ten Milky Way crossings it should thus contain a substantial amount of DM to avoid to have been entirely disrupted. Latest velocity dispersion measurements on M giant stars with 2MASS yields a light to mass ratio of about 25 [14]. The Sgr dSph core is positioned behind the bulge of Milky Way but outside the Galactic plane, thus reduced foreground γ -ray contaminations are expected. The luminous density profile of Sgr dSph has two components [15]. The compact component, namely the core, is characterized by a size of about 3 pc FWHM, which corresponds to a point-like region for H.E.S.S. This is the DM annihilation region from which γ -ray signal may be expected. A diffuse component is well fitted by a King model with a characteristic size of 1.6 kpc.

In this paper, we present the observation of the Sagittarius dwarf galaxy by the H.E.S.S. array of Imaging Atmospheric Cherenkov Telescopes based on a dataset collected in June 2006. A careful modeling of the Dark Matter halo using the latest measurements on the structural parameters of Sagittarius dwarf is presented to derive constraints on the WIMP velocity-weighted annihilation rate.

2 Search of VHE γ -rays from observations of Sagittarius Dwarf by H.E.S.S.

2.1 The H.E.S.S. instrument

H.E.S.S. (High Energy Stereoscopic System) is an array of four imaging atmospheric Cherenkov telescopes located in the Khomas Highlands of Namibia at an altitude of 1800 m above sea level. Each telescope consists of an optical reflector of about 107 m^2 effective area composed of 382 round mirrors arranged on a Davis-Cotton mount [16]. The interaction of the primary γ -ray in the Earth's upper atmosphere initiates an electromagnetic shower. The reflector collects the Cherenkov light emitted by the charged particles composing this shower, and focuses it onto a camera comprising 960 fast photomultipliers (PMTs) of individual field of view of 0.16° diameter [17]. Each tube is

equipped with Winston cones to limit the field of view of each PMT and minimize the background light. The total field of view of the H.E.S.S. instrument is 5° in diameter. The stereoscopy technique used in the imaging atmospheric Cherenkov telescopes allows for accurate reconstruction of the direction and energy of the primary γ -rays as well as an efficient rejection of the background induced by cosmic ray interactions [18]. The energy threshold of H.E.S.S. at zenith before selection cuts moved from 100 GeV at the commissioning of the experiment in 2003 to 160 GeV due to the degradation of the optical performance in 2006. The point source sensitivity is better than $2 \times 10^{-13} \text{cm}^{-2} \text{s}^{-1}$ above 1 TeV for a 5σ detection in 25 hours [19].

2.2 Dataset

The observations of the Sgr dSph were taken in June 2006 with zenith angles ranging from 7° to 43° around an average value of 19° . Data were taken in 28-minute observation runs in the wobble mode method with pointing directions offset by an angular distance of typically $\pm 0.7^\circ$ from the nominal target position. The dataset suitable for analysis was selected using the standard run selection procedure [19], which in particular removes the data taken under bad atmospheric conditions. A total of 25 runs out of 26 are selected for the analysis. After calibration of the raw shower images from PMT signals [20], two independent reconstruction techniques were combined to select γ -ray events and reconstruct their direction and energy. The first one uses the Hillas moment method [21]. The second analysis referred hereafter as “Model Analysis”, is based on the pixel-per-pixel comparison of the shower image with a template generated by a semi-analytical shower development model. The event reconstruction relies on a maximum likelihood method which uses available pixels in the camera, without requirement for an image cleaning [22,23]. The reconstructed shower parameter (energy, impact, direction and primary interaction point) are obtained as a product of the minimization procedure. The separation between γ candidates and hadrons is done using a combination of the Model goodness-of-fit parameter [23] and the Hillas mean scaled width and length parameters, which results in an improved background rejection [19]. Standard cuts on the width and the length of Hillas ellipses combined with the goodness-of-fit are used to suppress the hadronic background [21]. An additional cut on the primary interaction depth is used to improve background rejection. Both methods yield a typical energy resolution of 15% above energy threshold. In the Model Analysis, the angular resolution at the 68% containment radius is found to be better than 0.06° per γ -ray.

2.3 Data analysis

The on-source signal is defined by integrating all the events with angular position θ in a circle around the target position with a radius of θ_{cut} . The target position is chosen according to the photometric measurements of the Sgr dSph luminous cusp showing that the position of the centre corresponds to the centre of the globular cluster M54 [24]. The target position is thus found to be (RA = $18^h55^m59.9s$, Dec = $-30^d28'59.9''$) in equatorial coordinates (J2000.0) or ($l = 5^\circ41'12.9''$, $b = -14^\circ16'29.8''$) in Galactic coordinates. The signal coming from Sgr dSph is expected to come from a region of 1.5 pc, about $30''$, much smaller than the H.E.S.S. point spread function (PSF). A θ_{cut} value of 0.14° suitable for a point-like source was therefore used in the analysis. In case of a Navarro-Frenk-White (NFW) density profile [25] for which ρ follows r^{-1} or a cored profile [10] folded with the point spread function (PSF) of H.E.S.S., the integration region allows to retrieve a significant fraction of the expected signal. See Table 1. A cut on the image size of 60 photoelectrons is used to obtain a good sensitivity for weak sources. In order to reduce systematic effects which affect images close to the edges of the camera, only events reconstructed within a maximum distance of 2.5° from the camera centre are used for this analysis. The excess sky map is obtained by the subtraction of a background model on the γ -ray candidate sky distribution. The background level is estimated using the ring-background method [26] where the background rate is calculated from the integration of γ -like events falling in an annulus around the centre of the camera with identical observation conditions and acceptances than that used for the on-source region, which allows an estimate of the background on every sky position.

The excess sky map of the γ -ray candidates is presented in Fig. 1 in the RA/Dec J2000 coordinates centered on the Sgr target position. For each bin, γ -ray like events are summed within a radius of 0.14° . No γ -ray excess is found at the target position. Further, no significant excess is observed anywhere else in the sky map. The θ^2 distribution of the observed γ -ray events relative to the target position, is presented in Fig. 2 as well as the background distribution. In order to check the robustness of the results presented here, the dataset has been analyzed using different analysis methods as the so-called Hillas and model3D [27] methods. No significant γ -ray excess is detected in the corresponding sky maps.

Since Fig. 2 shows no γ -ray excess, we derived the 95% confidence level upper limit on the observed number of γ -rays : $N_\gamma^{95\% C.L.}$. The limit is computed knowing the numbers of events above the energy of 250 GeV in the signal region $N_{ON} = 437$, in the background region $N_{OFF} = 4270$, and the ratio of the off-source time to the on-source time $\alpha = 10.1$. We use the Feldman & Cousins method [28] and obtain :

$$N_\gamma^{95\% C.L.} = 56. \quad (1)$$

Given the acceptance of the detector for the observations of the dSph Sgr, an 95% confidence level upper limit on the γ -ray flux is also derived :

$$\Phi_\gamma(E_\gamma > 250 \text{ GeV}) < 3.6 \times 10^{-12} \text{ cm}^{-2} \text{ s}^{-1} \text{ (95\% C.L.)}$$

3 Predictions of γ -rays from Dark Matter annihilation

3.1 Theoretical framework

The annihilation of DM particles can generate γ -ray fluxes through different processes depending on the particle physics scenarios. Generally, WIMP annihilations will produce a continuum of γ -rays with energies up to the WIMP mass issued from the hadronization and decay of the cascading annihilation products, predominantly from π^0 's generated in the quark jets. In the R-parity conserving supersymmetric extensions of the Standard Model, the lightest supersymmetric particle (LSP) is a stable particle and is a good CDM candidate. The LSP is, in various SUSY breaking models, the lightest neutralino $\tilde{\chi}$. Being electrically neutral and colorless, it is among the best motivated candidates to account for CDM [29]. In Minimal Supersymmetric Standard Model (MSSM) scenarios [29], the annihilation of neutralinos can, on top of the hadronization continuum, produce also monoenergetic spectral lines of γ -rays resulting from loop-induced annihilation processes such as $\tilde{\chi}\tilde{\chi} \rightarrow \gamma\gamma$, $\tilde{\chi}\tilde{\chi} \rightarrow \gamma Z$, $\tilde{\chi}\tilde{\chi} \rightarrow \gamma h$, even though these are very challenging to detect experimentally due to the high suppression of such final states. Beyond the Standard Model, plausible candidates are provided by the universal extra dimension (UED) theories. In Kaluza-Klein (KK) scenarios with KK-parity conservation, the lightest Kaluza-Klein particle (LKP) is stable [30], the best-motivated being the first KK mode of the hypercharge gauge boson, $\tilde{B}^{(1)}$. In this case, $\tilde{B}^{(1)}$ pairs annihilate preferentially into charged lepton pairs which radiatively produce γ with harder spectra. Cascading decays of $q\bar{q}$ final states lead to secondary γ -rays [31].

The γ -ray flux from annihilations of DM particles of mass m_{DM} accumulating in a spherical DM halo can be expressed in the form :

$$\frac{d\Phi(\Delta\Omega, E_\gamma)}{dE_\gamma} = \frac{1}{4\pi} \underbrace{\frac{\langle\sigma v\rangle}{m_{DM}^2} \frac{dN_\gamma}{dE_\gamma}}_{\text{Particle Physics}} \times \underbrace{\bar{J}(\Delta\Omega)\Delta\Omega}_{\text{Astrophysics}} \quad (2)$$

as a product of a particle physics component with an astrophysics component. The particle physics part contains $\langle\sigma v\rangle$, the velocity-weighted annihilation cross section, and dN_γ/dE_γ , the differential γ -ray spectrum summed over the whole final states with their corresponding branching ratios. The astrophysical

part corresponds to the line-of-sight-integrated squared density of the DM distribution J , averaged over the instrument solid angle integration region for H.E.S.S. ($\Delta\Omega = 2 \times 10^{-5}$ sr) :

$$J = \int_{l.o.s} \rho^2(r[s]) ds \quad \bar{J}(\Delta\Omega) = \frac{1}{\Delta\Omega} \int_{\Delta\Omega} \text{PSF} * J d\Omega \quad (3)$$

where PSF is the point spread function of H.E.S.S.

3.2 Modeling the Sagittarius dwarf Dark Matter halo

The mass distribution of the DM halo of Sgr dwarf has been described by plausible models taking into account the best available measurements of the Sgr dwarf galactic structure parameters. We have used two widely different models. The first has a NFW cusped profile [25] with the mass density given by :

$$\rho_{NFW}(r) = \frac{A}{r(r + r_s)^2} \quad (4)$$

with A the normalization factor and r_s the scale radius taken from [10]. Using Eq. 3, the value of \bar{J} obtained with this model is reported in Table 1.

We have also studied a core-type halo model as in [10] characterized by the mass density :

$$\rho_{core}(r) = \frac{v_a^2}{4\pi G} \frac{3r_c^2 + r^2}{(r_c^2 + r^2)^2} \quad (5)$$

where r_c is the core radius and v_a a velocity scale. However, we have tried to update the v_a and r_c values which were used in [10]. By inserting in the Jeans equation the luminosity profile of the Sgr dwarf core of the form :

$$\nu(r) = \frac{\nu_0 r_c^{2\alpha}}{(r_c^2 + r^2)^\alpha} \quad (6)$$

we estimated from the data of reference [24] $\alpha = 2.69 \pm 0.10$ and $r_c = 1.5$ pc. Note that the value of r_c is only an upper limit. The value of the central velocity dispersion of Sgr Dwarf is $\sigma = 8.2 \pm 0.3 \text{ kms}^{-1}$ [32]. We have assumed that the velocity dispersion is independent of position. The value of v_a is then given by $v_a = \sqrt{\alpha} \sigma = 13.4 \text{ kms}^{-1}$. The cored model gives a very large value of \bar{J} , which is reported in Table 1. The third column of Table 1 gives the amount of signal expected in the solid angle integration region $\Delta\Omega = 2 \times 10^{-5}$ sr.

The value of \bar{J} in the cored model depends on various parameters such as the radial dispersion velocity, the baryon fraction in the core, the core radius and the velocity tensor anisotropy. The central value of the radial dispersion velocity was taken as 8.2 kms^{-1} . Previous measurements report 11.4 kms^{-1} [33] which would lead to an increase of a factor 4 in \bar{J} . Deviations from the asymptotically flat rotation curve have been studied. The effect of the α parameter

from [10] leads to a 50% increase or decrease in \bar{J} , according to the sign of α . The anisotropy in the velocity dispersion may lead to a reduction of a factor 2 in the dark matter density in the central region with respect to the case without anisotropy [34]. The baryon mass fraction in the very central region can not be neglected. However, the effect on \bar{J} turns out to be at most 50% due to the relatively fast increase of the mass-to-luminosity ratio with radius. Finally, in our model, the ratio of the luminous core radius to the dark matter core radius is $\rho = 1$. In general, as emphasized in [35], ρ could be lower than 1. \bar{J} is strongly dependent on the value of ρ . Extending the dark halo to 200 pc would lower \bar{J} by 2 orders of magnitude. Note also that our value of the luminous radius is only an upper limit. Decreasing the luminous radius leads to an increase of \bar{J} .

3.3 Sensitivity

For a given DM halo, the relevant quantities for DM particle annihilation searches are the DM particle mass m_{DM} and the velocity-weighted cross section $\langle\sigma v\rangle$. With the limit on the number of γ , N_γ , derived in section 2.4, we can compute the limit on $\langle\sigma v\rangle$ from H.E.S.S. results with the Sgr dwarf DM halo profile modeled in section 3.2. N_γ may be computed using the formula :

$$N_\gamma = T_{\text{obs}} \int_0^{m_{DM}} A_{\text{eff}}(E_\gamma) \frac{d\Phi(\Delta\Omega, E_\gamma)}{dE_\gamma} dE_\gamma \quad (7)$$

where A_{eff} corresponds to the effective area of the instrument obtained from Monte Carlo simulations as a function of the zenith angle, the offset of the source from the pointing direction, the energy of the event and the selection cuts. Using the expression of the differential flux given in Eq. 2 with Eq. 7 yields a 95% C.L. exclusion limit on the velocity-weighted cross section versus the DM particle mass for a given halo profile as defined by :

$$\langle\sigma v\rangle_{\text{min}}^{95\% \text{ C.L.}} = \frac{4\pi}{T_{\text{obs}}} \frac{m_{DM}^2}{\bar{J}(\Delta\Omega)\Delta\Omega} \frac{N_\gamma^{95\% \text{ C.L.}}}{\int_0^{m_{DM}} A_{\text{eff}}(E_\gamma) \frac{dN_\gamma}{dE_\gamma} dE_\gamma} \quad (8)$$

where dN_γ/dE_γ is computed with a parametrization of the differential continuum photon spectrum from [36] for a higgsino-type neutralino. Fig. 3 shows the limits in the case of a cored (green dashed line) and cusped NFW (red dotted line) profile using the value of \bar{J} computed in section 3.2. Predictions for phenomenological MSSM (pMSSM) models are displayed (grey points) as well as those satisfying in addition the WMAP constraints on the CDM relic density $\Omega_{\text{CDM}}h^2$ denoted as blue points. The values allowed by WMAP are taken to lie in the range $0.09 \leq \Omega_{\text{CDM}}h^2 \leq 0.11$. The SUSY models are calculated with DarkSUSY4.1 [37] in pMSSM framework and characterized by

a basic set of independent parameters : the higgsino mass parameter μ , the gaugino mass parameter M_2 , the CP-odd Higgs mass M_A , the common scalar mass m_0 , the trilinear couplings $A_{t,b}$ and the Higgs vacuum expectation value ratio $\tan\beta$. The set of parameters for a given model is randomly chosen in a parameter region encompassing a large class of pMSSM models, as described in Tab. 2.

In the case of a cusped NFW profile, the H.E.S.S. observations do not establish severe constraints on the velocity-weighted cross section. For a cored profile, due to a higher central density, stronger constraints are derived and some pMSSM models can be excluded in the upper part of the pMSSM scanned region.

In the case of KK dark matter, the differential γ spectrum is parametrized using Pythia [38] simulations and branching ratios from [30]. Predictions for the velocity-weighted cross section of $B^{(1)}$ dark matter particle are performed using the formula given in [39]. In this case, the expression for $\langle\sigma v\rangle$ depends analytically on the $B^{(1)}$ mass square. Fig. 4 shows the sensitivity of H.E.S.S. in the case of Kaluza-Klein models where the hypercharge boson $B^{(1)}$ is the LKP, for a cored (green solid line) and a cusped NFW (red solid line) profile respectively using the value of \bar{J} computed in section 3.2. With a NFW profile, no Kaluza-Klein models can be tested. In the case of a cored model, some models providing a LKP relic density compatible with WMAP constraints can be excluded. From the sensitivity of H.E.S.S., we derive a lower limit on the $B^{(1)}$ mass of 500 GeV.

4 Discussion

The Sgr dSph galaxy is among the best target to search for DM signal. Sgr dSph region is devoid of astrophysical background unlike the Galactic Center region. Indeed, the presence of several γ -ray emitters and diffuse emission makes difficult to disentangle the emission from the very center from that of other objects. The absence of gas in Sgr offers a cleaner environment to search for γ -ray emission.

The DM profile uncertainties for Sgr dSph are about one order of magnitude. In contrast, the Milky Way DM profile suffers from large uncertainties, up to five orders of magnitude, due to the difficulty of measuring the structural parameters of our Galaxy in the central 10^{-2} pc.

A modest observation time allows us for the first time to test some pMSSM models for the γ -ray annihilation of neutralinos in the direction of Sgr dSph. Some KK models can already be excluded.

Sgr dSph is a target for deeper observations by H.E.S.S. With 100 hours, H.E.S.S. will be able to test pMSSM models assuming a NFW profile. With such an observation time, H.E.S.S. could exclude all the cosmologically allowed

KK models in case of a core profile.

5 Conclusion

The observations of the Sagittarius dwarf spheroidal galaxy with H.E.S.S. performed in June 2006 reveal no significant γ -ray excess at the nominal target position. The Sagittarius dwarf dark matter halo has been modeled using latest measurements of its structure parameters. Constraints have been derived on the velocity-weighted cross section of the dark matter particle in the framework of supersymmetric and Kaluza-Klein models.

Acknowledgements: The support of the Namibian authorities and of the University of Namibia in facilitating the construction and operation of H.E.S.S. is gratefully acknowledged, as is the support by the German Ministry for Education and Research (BMBF), the Max Planck Society, the French Ministry for Research, the CNRS-IN2P3 and the Astroparticle Interdisciplinary Programme of the CNRS, the U.K. Particle Physics and Astronomy Research Council (PPARC), the IPNP of the Charles University, the South African Department of Science and Technology and National Research Foundation, and by the University of Namibia. We appreciate the excellent work of the technical support staff in Berlin, Durham, Hamburg, Heidelberg, Palaiseau, Paris, Saclay, and in Namibia in the construction and operation of the equipment. We thank Edmond Giraud for suggestions and discussions concerning the Sagittarius Dwarf Galaxy observations by H.E.S.S.

References

- [1] G. Bertone, D. Hooper, J. Silk, Phys. Rep. **405** (2005) 279
- [2] E. Baltz *et al.*, Phys. Rev. **D61** (2000) 023514
- [3] F. A. Aharonian *et al.* (H.E.S.S. collaboration), Science **314** (2006) 1424
- [4] N. Fornengo *et al.*, Phys. Rev. **D70** (2004) 103529
- [5] A. Tasitsiomi *et al.*, Astropart. Phys. **21** (2004) 637
- [6] F. A. Aharonian *et al.* (H.E.S.S. collaboration), Phys. Rev. Lett. **97** (2006) 221102
- [7] C. van Eldik *et al.*, Proc. of the 30th International Cosmic Ray Conference, Merida, 2007
- [8] F. A. Aharonian *et al.* (H.E.S.S. collaboration), Nature **439** (2006) 695
- [9] F. A. Aharonian & A. Neronov, Astrophys. J. **619** (2005) 306
- [10] N. W. Evans, F. Ferrer and S. Sarkar, Phys. Rev. **D69** (2004) 123501
- [11] M.I. Wilkinson *et al.*, Proc. of XXIst IAP Colloquium : Mass Profiles & Shapes of Cosmological Structures, Paris, 2005
- [12] R. Ibata , G. Gilmore, M. Irwin, MNRAS **277** (1995) 781
- [13] S. Majewski *et al.*, Astrophys. J. **599** (2003) 1082
- [14] S. Majewski *et al.*, Proc. of the IAU Symposium 220: Dark Matter in Galaxies, Sydney, 2003
- [15] L. Monaco *et al.*, MNRAS **356** (2006) 1396
- [16] K. Bernlöhner, O. Carrol, R. cornils *et al.*, Astropart. Phys. **20** (2003) 111
- [17] P. Vincent *et al.*, Proc. of the 28th International Cosmic Ray Conference, T. Kajita *et al.*, (Eds. Universal Academy Press, Tokyo, 2003), 2887
- [18] S. Funk *et al.*, Astropart. Phys. **22** (2004) 285
- [19] F. A. Aharonian *et al.* (H.E.S.S. collaboration), A&A **457** (2006) 899
- [20] F. A. Aharonian *et al.* (H.E.S.S. collaboration), Astropart. Phys. **22** (2004) 109
- [21] F. A. Aharonian *et al.* (H.E.S.S. collaboration), A&A **430** (2005) 865
- [22] M. de Naurois *et al.*, Proc. of 28th ICRC, Vol 5 (2003) 2907
- [23] M. de Naurois *et al.*, Proc. of Towards a Network of Atmospheric Cherenkov Detectors, Palaiseau, 2005
- [24] L. Monaco, M. Bellazzini, F.R. Ferraro and E. Pancino, MNRAS **356** (2005) 1396

- [25] J. Navarro, C. Frenk and S. White, *Astrophys. J.* **490** (1997) 493
- [26] G. Pühlhofer *et al.*, *Astropart. Phys.* **20** (2003) 267
- [27] M. Lemoine-Goumard, B. Degrange, M. Tluczykont, *Astropart. Phys.* **25** (2006) 195
- [28] G. Feldman & R. Cousins, *Phys. Rev.* **D57** (1998) 3873
- [29] G. Jungman, K. Kamionkowski, K. Griest, *Phys. Rep.* **276** (1996) 195
- [30] G. Servant & T. Tait, *Nucl. Phys.* **B650** (2003) 391
- [31] L. Bergström *et al.*, *Phys. Rev. Lett.* **94** (2005) 131301
- [32] S. Zaggia *et al.*, *Mem. Soc. Astr. It. Suppl.* **5** (2004) 291
- [33] R. Ibata *et al.*, *Astron. J.* **113** (1997) 634
- [34] D. Merritt, *Astron. J.* **95** (1988) 2
- [35] C. Pryor & J. Kormendy, *Astron. J.* **100** (1990) 1
- [36] L. Bergström, P. Ullio and J. Buckley, *Astropart. Phys.* **9** (1998) 137
- [37] P. Gondolo *et al.*, *JCAP* **0407** (2004) 008
- [38] PYTHIA package
- [39] E. Baltz & D. Hooper, *JCAP* **0507** (2005) 001

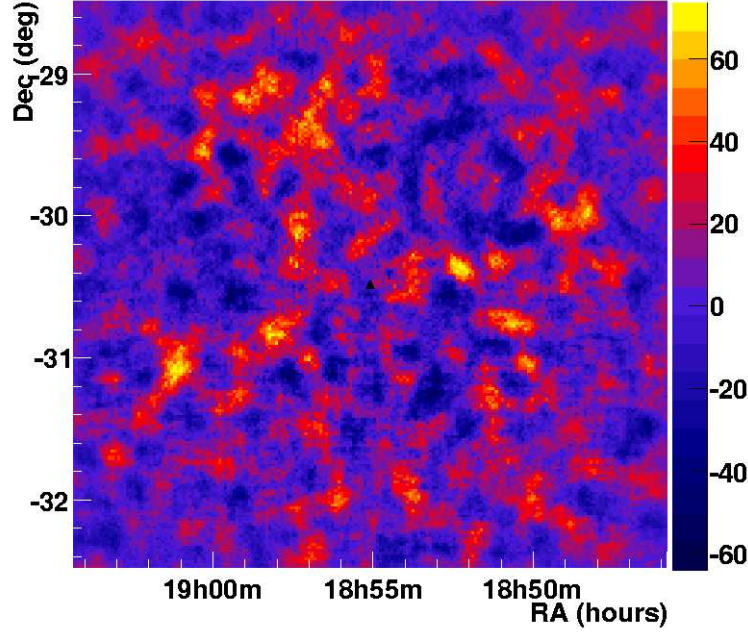


Fig. 1. Sky map of the γ -ray candidates with an oversampling radius of 0.14° . No excess is observed at the target position (RA = 18h54m40s, Dec = $-30^\circ 27' 05''$) in equatorial coordinates (J2000) marked with a black triangle. Other spots in the field of view are not significant.

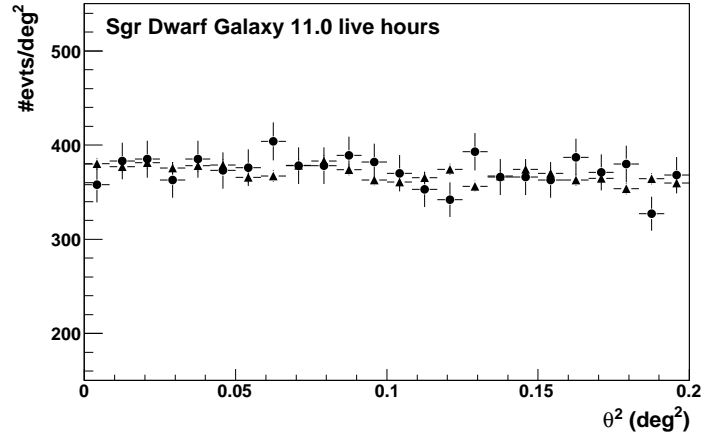


Fig. 2. θ^2 radial distribution of the ON and OFF events for γ -ray like events from the target position (RA = 18h54m40s, Dec = $-30^\circ 27' 05''$) (black dots). Estimated background calculated as explained in the text is shown (black triangles). No excess is seen at small θ^2 value.

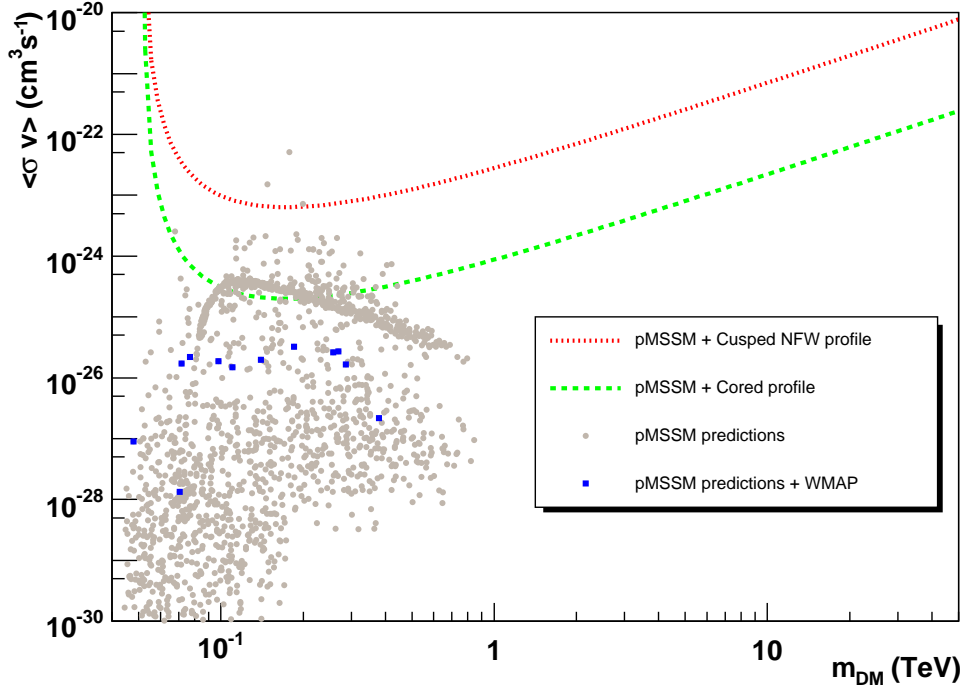


Fig. 3. Upper limits at 95% C.L. on $\langle\sigma v\rangle$ versus the DM particle mass in the case of a cusped NFW (red dotted line) and a cored (green dashed line) DM halo profiles respectively. The pMSSM parameter space was explored with DarkSUSY 4.1 [37], each point on the plot corresponding to a specific model (grey point). Amongst these models, those satisfying in addition the WMAP constraints on the CDM relic density are overlaid as blue square (see text for details). The limits in case of neutralino dark matter from pMSSM are derived using the parametrisation from reference [36] for a higgsino type neutralino annihilation γ profiles.

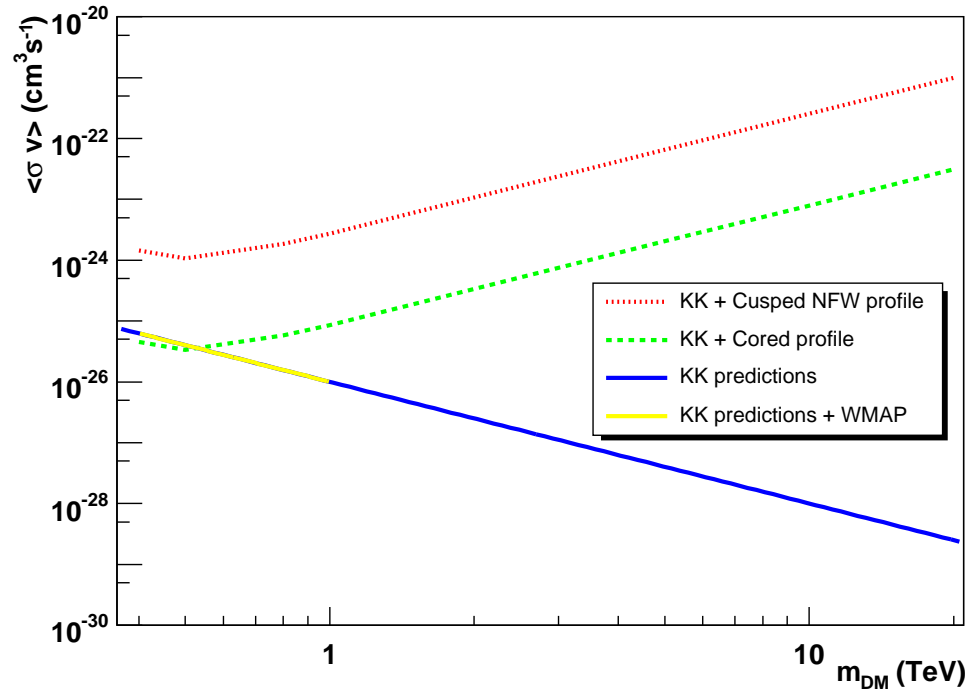


Fig. 4. Upper limits at 95% C.L. on $\langle\sigma v\rangle$ versus the DM particle mass in the $B^{(1)}$ Kaluza-Klein scenarios for a cusped NFW (red dotted line) and a cored (green dashed line) DM halo profiles respectively. The blue line corresponds to Kaluza-Klein models [30]. Overlaid (yellow line) are the KK models satisfying WMAP constraints on the CDM relic density (see text for details).

Table 1

Structural parameters for a cusped NFW (r_s, A) and a cored (r_c, v_a) DM halo model, respectively. The values of the solid-angle-averaged l.o.s integrated squared DM distribution are reported in both cases for the solid angle integration region $\Delta\Omega = 2 \times 10^{-5}\text{sr}$.

Halo type	Parameters	\bar{J} ($10^{24}\text{GeV}^2\text{cm}^{-5}$)	Fraction of signal in $\Delta\Omega = 2 \times 10^{-5}\text{sr}$
Cusped NFW halo	$r_s = 0.2 \text{ kpc}$ $A = 3.3 \times 10^7 M_\odot$	2.2	93.6%
Cored halo	$r_c = 1.5 \text{ pc}$ $v_a = 13.4 \text{ km s}^{-1}$	75.0	99.9%

Table 2

Region of the pMSSM parameter space randomly scanned to generate the models. A set of free parameters in the considered ranges corresponds to a pMSSM model.

pMSSM parameter space region
$100 \text{ GeV} \leq \mu \leq 30 \text{ TeV}$
$100 \text{ GeV} \leq M_2 \leq 50 \text{ TeV}$
$50 \text{ GeV} \leq M_A \leq 10 \text{ TeV}$
$100 \text{ GeV} \leq m_0 \leq 1 \text{ TeV}$
$-3 \text{ TeV} \leq A_t \leq 3 \text{ TeV}$
$-3 \text{ TeV} \leq A_b \leq 3 \text{ TeV}$
$1.2 \leq \tan \beta \leq 60$

List of Figures

- 1 Sky map of the γ -ray candidates with an oversampling radius of 0.14° . No excess is observed at the target position (RA = 18h54m40s, Dec = $-30^\circ 27' 05''$) in equatorial coordinates (J2000) marked with a black triangle. Other spots in the field of view are not significant. 16
- 2 θ^2 radial distribution of the ON and OFF events for γ -ray like events from the target position (RA = 18h54m40s, Dec = $-30^\circ 27' 05''$) (black dots). Estimated background calculated as explained in the text is shown (black triangles). No excess is seen at small θ^2 value. 16
- 3 Upper limits at 95% C.L. on $\langle\sigma v\rangle$ versus the DM particle mass in the case of a cusped NFW (red dotted line) and a cored (green dashed line) DM halo profiles respectively. The pMSSM parameter space was explored with DarkSUSY 4.1 [37], each point on the plot corresponding to a specific model (grey point). Amongst these models, those satisfying in addition the WMAP constraints on the CDM relic density are overlaid as blue square (see text for details). The limits in case of neutralino dark matter from pMSSM are derived using the parametrisation from reference [36] for a higgsino type neutralino annihilation γ profiles. 17
- 4 Upper limits at 95% C.L. on $\langle\sigma v\rangle$ versus the DM particle mass in the B⁽¹⁾ Kaluza-Klein scenarios for a cusped NFW (red dotted line) and a cored (green dashed line) DM halo profiles respectively. The blue line corresponds to Kaluza-Klein models [30]. Overlaid (yellow line) are the KK models satisfying WMAP constraints on the CDM relic density (see text for details). 18

List of Tables

- 1 Structural parameters for a cusped NFW (r_s, A) and a cored (r_c, v_a) DM halo model, respectively. The values of the solid-angle-averaged l.o.s integrated squared DM distribution are reported in both cases for the solid angle integration region $\Delta\Omega = 2 \times 10^{-5}\text{sr}$. 19

- 2 Region of the pMSSM parameter space randomly scanned to generate the models. A set of free parameters in the considered ranges corresponds to a pMSSM model. 19